AIAA JOURNAL
Vol. 48, No. 12, December 2010

Validation of a Zonal Approach Computing the Sound Radiation from Lined Ducts

Clemens Buske*
DLR, German Aerospace Center, 37073 Göttingen, Germany
Christoph Richter† and Frank Thiele‡
Technical University of Berlin, 10623 Berlin, Germany
Chao Yu§
PPG Industries, Cheswick, Pennsylvania 15024
and
Mei Zhuang¶
Ohio State University, Columbus, Ohio 43210-1276

DOI: 10.2514/1.J050478

A zonal approach for the prediction of the far-field radiation from flows in lined ducts is investigated. The approach combines a high-order computational aeroacoustics scheme with the recently developed acoustic intensity-based method for the calculation of far-field radiations. The advantage over the application of an acoustic analogy is the usage of an open control surface for the acoustic input. The capability of the current hybrid approach was validated on the basis of two benchmark cases. One considers the sound radiation from a two-dimensional semi-infinite duct in which a small fraction of the walls close to outlet nozzle is lined. The second problem concerns the sound radiation from a bypass enginelike annular duct with lined and hardwalled configurations of the infinite centerbody and sheared flow conditions. A broadband time-domain impedance boundary condition based on the extended Helmholtz resonator model and the Ingard–Myers boundary condition is implemented in the computational aeroacoustic code to model the acoustic linings. Although mesh refinement may improve the solutions, the good agreements of analytical solutions and numerical results, in particular for the radiation characteristics, verify this approach as an accurate and efficient prediction tool.

Nomenclature

c	=	speed of sound
D_n	=	directivity factor
f	=	frequency
$f_* = f\frac{H}{c}$	=	reduced frequency
$\mathcal{G}_n$	=	spherical Hankel function
$\mathcal{H}_n$	=	Hankel function
$i = \sqrt{-1}$	=	imaginary unit
k	=	wave number ω/c
Ma	=	Mach number
m_{EHR}	=	face reactance
n	=	y-mode number/radial mode number
$\mathbf{n}$	=	unit normal vector
P	=	pressure perturbation in frequency domain
$\mathcal{P}_n^m$	=	associated Legendre polynomial
p_0	=	ambient pressure
p'	=	pressure perturbation
R	=	acoustic resistance
R_i	=	acoustic intensity-based method's input surface radius
R_o	=	acoustic intensity-based method's observer surface radius
(r, ϑ)	=	polar coordinates
(r, ϑ, φ)	=	spherical coordinates
T_l	=	extended Helmholtz resonator's period time
$\mathbf{u}_0$	=	mean velocity vector
u_n'	=	normal velocity perturbation
(x, y, z)	=	Cartesian coordinates
Z_w	=	complex acoustic wall impedance
β	=	cavity reactance
$\gamma = \sqrt{1 - Ma^2}$	=	Prandtl–Glauert factor
ε	=	cavity resistance
κ	=	ratio of specific heats
$\mu(t)$	=	Myers term
ρ_0	=	ambient density
ω	=	angular frequency
∇	=	nabla operator

Presented as Paper 2009-3169 at the 15th AIAA/CEAS Aeroacoustics Conference (30th AIAA Aeroacoustics Conference), Miami, FL, 11–13 May 2009; received 4 February 2010; revision received 29 July 2010; accepted for publication 10 August 2010.

*Graduate Engineer, Institute of Propulsion Technology, Bunsenstrasse 10. Student Member AIAA.

†Graduate Engineer, Institute of Fluid Mechanics and Engineering Acoustics, Müller-Breslau-Strasse 8. Student Member AIAA.

‡Professor, Institute of Fluid Mechanics and Engineering Acoustics, Müller-Breslau-Strasse 8. Member AIAA.

§Senior Development Engineer, GDBC, 400 Guys Run Road. Member AIAA.

¶Professor, Department of Mechanical and Aerospace Engineering, 201 West 19th Avenue. Associate Fellow AIAA.

I. Introduction

AN EVALUATION of acoustic radiations in both the near- and the far-fields from an aeroengine using a single numerical method is still out of reach for current numerical resources. It is therefore critical to develop a practical zonal approach that combines different numerical methods for different flow regions through which the acoustic waves propagate. In the current study, a state-of-the-art zonal approach is presented and validated with published analytical solutions for the acoustic radiation from lined flow ducts. The idea of using a hybrid approach for such a problem is not entirely new; it started with Hardin and Lemkin [1], who considered the combination of a classical computational fluid dynamics (CFD) method with an acoustic analogy for the far-field prediction. It has been followed by a

number of applications, which combine far-field prediction methods, such as the Ffowcs–Williams and Hawkings (FWH) integral method with a computational aeroacoustic (CAA) method [2,3]. However, two critical challenges arise when the time-domain impedance boundary condition with mean flow and the radiation through a free shear layer are included in the prediction of far-field acoustic radiations from an aeroengine. Namely, the Kelvin–Helmholtz instability of the shear layers disturbs the solution. New ideas and implementations for the practical handling of such challenges are developed and validated in the current work.

Although significant advances have been made in the modeling of the noise generation and propagation, there are still several essential issues that need to be resolved in order to establish the methods in an industrial environment. One of them is an efficient description of an acoustic lining under flow conditions in the time domain, including the modeling of the flow effect on the impedance without an extensive mesh refinement for the wall-bounded shear layer. The time-domain impedance boundary conditions have been studied extensively in the past decade. Some interesting and new ideas have been added to the time-domain impedance models, which allow the implementation of likewise impedance models to a broad spectrum of numerical methods. The latest development of a broadband time-domain impedance model, namely, the extended Helmholtz resonator (EHR) model [4], has been successfully implemented into a CAA method [5–7], and the method is being validated here as part of the hybrid zonal approach for the computation of the acoustic far-field radiation.

Two further essential issues for the applicability of a zonal approach to a realistic aeroengine are related to the jet formed by flows from the bypass duct. First, the free shear layer between the bypass flow and external stream can refract the sound waves radiated to the far field. This phenomenon is described in the analytical solution by an interface condition similar to the boundary condition of Ingard–Myers for the impedance surface. In fact, there may also be a strong nonlinear interaction of sound waves and turbulence in the shear layer, which is neglected here for stability reasons. The second issue is the instability problem when solving the linearized Euler equations numerically over a resolved thin shear layer. This problem is addressed by a filtering of the sheared mean flow profile in order to remove the instability by artificially thickening the profile.

The existence of the shear layer also adds an essential practical problem for the traditional far-field integral methods. Because of the inhomogeneous base flow properties over the shear layer, the assumption of constant conditions outside the integration surface, which are used for most of the far-field integral methods, is inevitably violated. In addition, the integration surface that encloses the sound source region must be closed for a classical far-field integration method, such as the Kirchoff and FWH. The presence of a shear layer, therefore, results in errors with these methods. A recently developed acoustic intensity-based method (AIBM) [8] is employed in this study for the acoustic far-field prediction. The AIBM is an asymptotic method that directly solves the far-field prediction using an inverse problem technique. Although the AIBM also requires the sound waves to propagate in a homogeneous medium outside the control surface, it only needs acoustic input data from an open control surface as opposed to the closed FWH surface. The computational accuracy and efficiency in aeroacoustic problems have been demonstrated by Yu et al. [9,10]. The present validation confirms the effectiveness for the hybrid method on the whole for two-dimensional (2-D) as well as axisymmetric geometries with lined duct walls and shear flow conditions.

This paper is organized as follows. In Sec. II, the basic implementation principles of the two numerical methods are summarized. The CAA method used for the near-field computation is described first, with particular interest in the modeling of the linings using the EHR, followed by a brief depiction of the AIBM as a far-field method. In Sec. III, the two benchmark problems are presented, the settings of the zonal methods are given, and the numerical results are compared with the analytical solutions. The conclusions are drawn in Sec. IV.

II. Numerical Methods

A. Computational Aeroacoustic Method

The radiation of single tones and modes, as well as the broadband radiation from lined flow ducts of an aeroengine, is one of the major perspective applications of high-order CAA methods. Even though such high-order CAA methods could also be used to calculate the observed sound pressure level (SPL) in the duct, the near field of the duct exit, and even the moderate far field, this seems highly inefficient in terms of computational time and numerical accuracy. Therefore, a CAA method is applied here to compute the sound propagation inside the flow duct and to the near field only. The linearized Euler equations over an arbitrary mean flow are solved numerically using the dispersion-relation-preserving (DRP) finite difference scheme [11] and a low-dissipation and dispersion Runge–Kutta scheme as a $2N$ storage variant, proposed by Stanescu and Habashi [12]. Spurious waves are suppressed by an 11-point filter deployed every other time step.

The acoustic linings are addressed by a time-domain impedance boundary condition, which is going to be validated and benchmarked in the current work. The impedance model is based on the EHR model of Rienstra [4]. It has been implemented and validated with a CAA method [13,14] that is capable of handling 2-D problems, including Cartesian and modal axisymmetric ones, as well as three-dimensional (3-D) problems. The impedance boundary condition has been validated with experiments, and the numerical properties have been extensively investigated [5–7].

The frequency response of the impedance is described by the five parameter EHR model [4] as

$$Z_w = R + i\omega m_{\mathrm{EHR}} - i\beta \cot(\tfrac{1}{2}\omega T_l - i\tfrac{1}{2}\varepsilon) \tag{1}$$

The time-domain impedance boundary condition is given by

$$\frac{\partial u_n'}{\partial t}(t) = \frac{1}{m_{\mathrm{EHR}}}[\mu(t) - e^{-\varepsilon}\mu(t-T_l) - (R+\beta)u_n'(t) + (R-\beta)e^{-\varepsilon}u_n'(t-T_l)] + e^{-\varepsilon}\frac{\partial u_n'}{\partial t}(t-T_l) \tag{2}$$

wherein the mean flow effects are considered in $\mu(t)$ according to the Myers boundary condition [15]:

$$\mu(t) := p' + \mathbf{u}_0 \cdot \nabla\tilde{p}' - \mathbf{n} \cdot (\mathbf{n} \cdot \nabla\mathbf{u}_0)\tilde{p}' \tag{3}$$

with

$$p' = \frac{\partial\tilde{p}'}{\partial t} \tag{4}$$

A more detailed description of this implementation can be found in Richter et al. [7].

The mean flow conditions of the second investigated problem include an infinite thin sheared mean flow profile with a thermal boundary layer that cannot be handled by the current CAA method. As described previously, the related model in the frequency domain is similar to the Ingard–Myers boundary condition and adds an instability when transferred to the time domain. A repeated filtering of the base flow and source variables with a second-order Taylor filter is introduced. The filtering results in an artificially thickened shear layer profile. In addition, due to the low-order filtering of the mean flow gradients, which acts as the source terms here, the stability is greatly improved.

B. Acoustic Intensity-Based Method

The AIBM is recently developed for the far-field prediction [8–10]. The method expresses the solution of the Helmholtz equation in an asymptotic form of a linear combination of basis functions. The 2-D asymptotic solution of Helmholtz with mean flow in x direction is written as [10]

$$P(x,y) = \exp(ikMa\hat{x}/\gamma)\Bigg[a_0\mathcal{H}_0(k\hat{r}/\gamma) + \sum_{n=1}^{N}(a_n\cos n\hat{\vartheta} + b_n\sin n\hat{\vartheta})\mathcal{H}_n(k\hat{r}/\gamma)\Bigg] \quad (5)$$

The axisymmetric formulation is simplified from 3-D asymptotic expression with mean flow in the z direction, which can be written as [9]

$$P(x,0,z) = \exp(ikMa\hat{z}/\gamma^2)\sum_{n=0}^{N}\sum_{m=0}^{n}[a_{nm}\xi_m - ib_{nm}\eta_m]\mathcal{Q}_n^m(\hat{z}\hat{r}^{-1})\mathcal{G}_n(k\gamma\hat{r}^{-1})/(2\hat{r}^m) \quad (6)$$

where

$$\xi_m = (\hat{x}+i\hat{y})^m + (\hat{x}-i\hat{y})^m, \qquad \eta_m = (\hat{x}+i\hat{y})^m - (\hat{x}-i\hat{y})^m \quad (7)$$

and $\mathcal{Q}_n^m = \mathcal{P}_n^m/\sin^m\hat{\varphi}$, amd $(\hat{x},\hat{y},\hat{z}) = (\gamma x, \gamma y, \gamma z)$. N is a suitable integer. The choice for N has been discussed in [9]. One obvious restriction is that the number of coefficients to be determined must be less than the number of the measurement or input points. The coefficients a_n and b_n or a_{nm} and b_{nm} are determined by solving the inverse problem $\mathbf{A}x = \mathbf{b}$ with boundary conditions of pressure and its normal derivative over an open surface in a radiated field. Then the entire radiated field can be calculated efficiently as a direct problem. The theoretical uniqueness of the solution is guaranteed by the unique continuation theory of elliptic equations. Although the method is stated in frequency domain, it effectively predicts acoustic radiation of multiple frequencies through superposition. AIBM combined with CFD and/or CAA is particularly effective for the prediction of far-field aeroacoustic noise. AIBM requires acoustic input data from only an open surface as opposed to the closed FWH surface required by conventional methods, and it is extremely efficient for 3-D aeroacoustic applications. AIBM can also be used under the presence of inhomogeneous mean flows, and thus provides an effective alternative for far-field prediction of aeroacoustic problems.

III. Validation of the Hybrid Method

A. Radiation of Sound from a Two-Dimensional Acoustically Lined Duct

Figure 1 shows the geometry of the 2-D duct problem that was presented by Koch [16]. A semi-infinite parallel plate channel of height H is equipped with a finite-length lining panel of length L_l. The lining section is located a distance L_s away from the open end of the duct. Koch simplifies the problem by abstracting walls to be infinitely thin. This assumption is also used in this numerical investigation. A sound source on the outer left side of the computation domain, shown in Fig. 1, generates a sound wave of amplitude $\hat{p}_n$, wherein n denotes the mode number in the y direction. The wave oscillates with different frequencies, given as reduced frequencies $f_* = f\frac{H}{c}$. Following the notation of Koch, the reduced frequency is used here synonymously for the Helmholtz number $He = \frac{H}{\lambda}$. The sound wave impinges on the lined section and is partly reflected and absorbed before it is radiated from the duct end. In the outside region to the right, only outgoing waves exist and determine the directivity

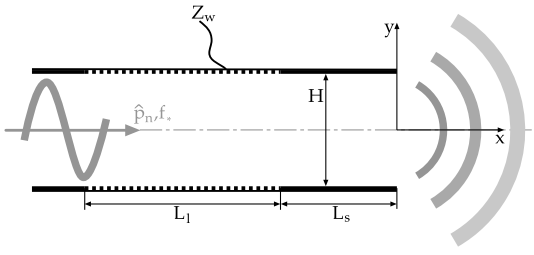

Fig. 1 Geometry of the 2-D duct problem.

Table 1 Studied cases of the 2-D lined and hardwalled duct configurations

	Reduced frequency f_*				
y mode n	0.2	0.8	1.2	1.8	2.8
0	N0-F0.2	N0-F0.8		N0-F1.8	N0-F2.8
1		N1-F0.8		N1-F1.8	N1-F2.8
2			N2-F1.2	N2-F1.8	N2-F2.8

characteristics. Table 1 names the cases that are computed, compared with Koch's results and consulted for the validation.

For each frequency, Koch analyzed the lined as well as the completely hardwalled duct configuration. Koch [16] applied an impedance model of Ko [17], which is very similar to the current EHR model. Moreover, the relation of the geometry of the single-layer classical Helmholtz resonator-type liner to its impedance is provided by Koch [16] in terms of a specific face sheet reactance frequency scale f_{0*}, reduced cavity depth d_*, resistance parameter R_*, and their relation to the internal structure as

$$Z_w = R_*\left(1 + i\frac{f_*}{f_{0*}}\right) - i\cot(2\pi f_* d_*) \quad (8)$$

The parameters of the EHR [Eq. (1)] can simply be identified with the parameters used in Koch's publication by comparison of the coefficients. The second parameter, the if_* term, corresponds to a very small mass reactance of the EHR ($m_{\mathrm{EHR}} = 1.5\times10^{-5}$), and hence leads to a very small time-step size. The validation is carried out for several frequencies individually while the EHR parameters are kept constant. Therefore, the validation can be considered a validation of the broadband capabilities of the boundary condition as well.

Table 2 summarizes the physical parameters employed in this study. The last three parameters were taken from the U.S. Standard Atmosphere [18] at sea level, while the ratio of specific heats κ is set for an idealized gas with two atoms.

1. *Computational Aeroacoustic Method Configuration*

The computation domain of the CAA method is divided into eight rectangular subdomains for a parallelized computation (see Fig. 2). The duct itself, which is located in the center of the figure, is split into three subdomains according to the wall boundaries: the hardwalled duct inlet (I), the sound-absorbing lining section (II), and the hardwalled duct outlet (III). Sound waves of 130 dB enter the computational domain at the nonreflecting sound source boundary in block I. At the transition to the ambient free field, a radiation boundary condition according to Bogey and Bailly [19] is applied, giving only little reflections and no instabilities from the domain's border regions. The uniform grid accommodates 30 grid spacings in a vertical direction inside the duct. In only the lining section (II) and the duct section (I), the grid was slightly stretched with a factor of

Table 2 Parameters of the 2-D lined duct problem by Koch [16]

Quantity	Value	Description
H	187.3 mm	Duct height
L_s	$2.17H$	Distance of the lining section from the duct exit
L_l	$1H$	Length of the lining section
$R_* = R/(\rho_0 c)$	1.4	Specific acoustic resistance
$f_{0*} = f_0 H/c$	8.14	Reduced characteristic frequency of the facing sheet material
$d_* = d/H$	0.136	Dimensionless depth of the honeycomb cavities
κ	1.4	Ratio of specific heats
c	340.29 m/s	Speed of sound
p_0	101,325 Pa	Ambient pressure
ρ_0	1.2250 kg/m^3	Ambient density

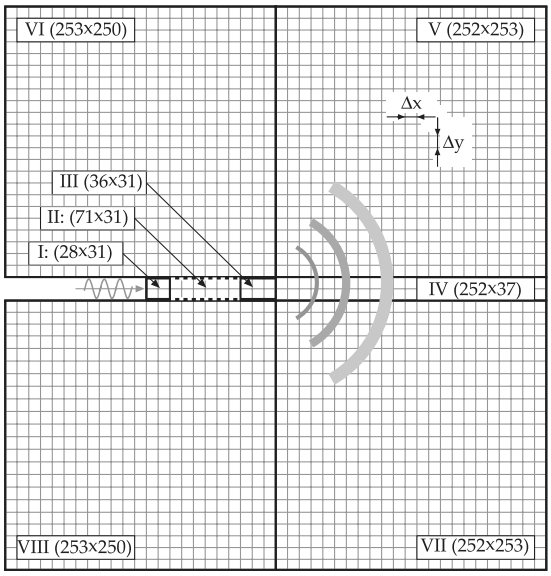

Fig. 2 CAA computation domain of the 2-D duct problem.

1.0016 in the x direction to fit the liner's length. Altogether, the highest frequency is resolved with 10.7 points per wavelength (PPW), and the total number of grid points is about 270,000.

As previously mentioned, the small mass reactance dictates the small time step of $\Delta t = 5.5 \cdot 10^{-8}$ s to obtain a stable solution with the time-optimized alternating 5–6-stage Runge–Kutta scheme. The comparative cases where the acoustic linings are replaced by a hard wall are executed with an increased time step of $\Delta t = 8.9 \cdot 10^{-7}$ s. The computations were carried out on four 2.2 GHz Advanced Micro Devices, Inc. (AMD) Opterons. Statistical stationarity is achieved within 40,000 iterations, taking 12 h, and within 360,000 iterations, taking 112 h, for the hardwalled and the partially lined cases, respectively.

2. *Acoustic Intensity-Based Method Configuration*

The intensity-based far-field computation is based on the CAA data that are interpolated on a semicircle of radius R_i and its center located at the duct exit. The pressure gradient in the direction normal to this control surface is approximated of the second order. The far field can be computed on an arbitrary 2-D domain, although a second concentric semicircle line of radius R_o is sufficient as an observer surface, in this case, for comparison with Koch's results [16]. Figure 3 depicts the CAA computation domain and the AIBM input and observer surfaces. To determine the optimal control surface for an efficient and accurate far-field prediction, preliminary studies in modifying the control surface radius and the number of surface points were carried out [20]. The evaluation is based on the comparison of the AIBM's reconstructed field on an observer surface inside the CAA domain, with the original CAA data at this distance.

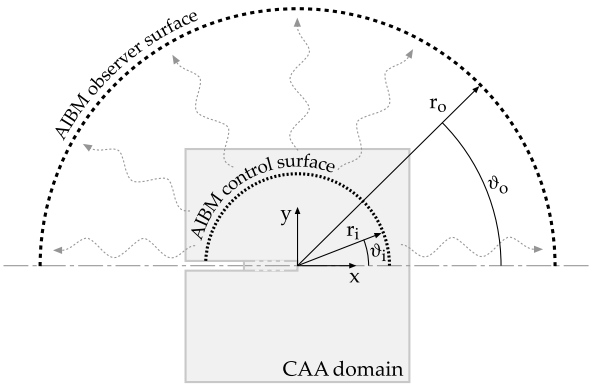

Fig. 3 AIBM control and observer surfaces of the 2-D duct problem.

The accumulated deviations are weighted by the number of surface points to give respect to different amounts of surface points. A good compromise in terms of time and accuracy is achieved with the largest possible control surface radius of $R_i = 1.5$ m and 980 equally spaced surface points. The AIBM far-field surface has no impact on the far-field computation itself, only the resolution of the solution is affected. For a continuous and representative far-field solution, the semicircle observer surface was designed at a distance $R_o = 50$ m away from the duct exit, consisting of 500 equidistant surface points. The AIBM computations were carried out on a 2.13 GHz Intel Core 2 Duo E6420 PC. Each computation for the hardwalled and the lined configurations took between 1.2 and 1.8 s.

3. *Results*

For each mode and frequency, Koch's results [16] (which are based on the Wiener–Hopf technique) are compared with the CAA and the AIBM solutions simultaneously. Figures 4–6 show the space-independent directivity factor D_n,

$$D_n = \frac{p_{\text{rms,far-field}}\sqrt{R_o/H}}{p_{\text{rms,incoming}}} \tag{9}$$

of the fundamental, as well as of the first antisymmetric and symmetric incoming duct waves with modes $n = 0$, 1, and 2. The upper half planes show the hardwalled cases, while the cases with linings are depicted in the lower half planes.

The current hybrid zonal approach shows good agreement with the directivity patterns of Koch [16], in particular at low frequencies. At higher frequencies, and mostly at small radiation angles $\vartheta < 20°$, the

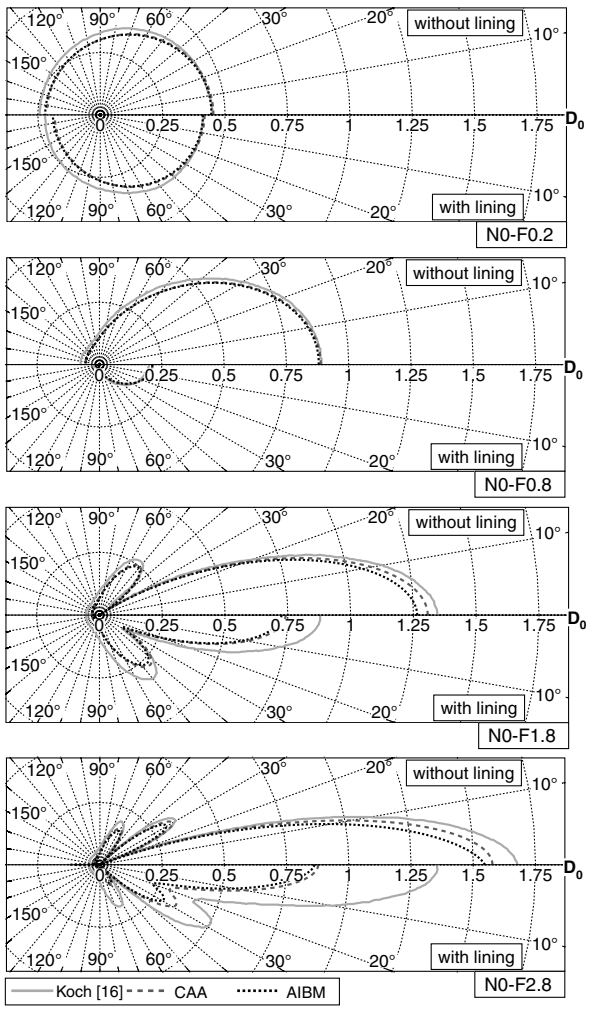

Fig. 4 Directivity factors of the fundamental mode D_0 [Eq. (9)]; from top to bottom, $f_* = 0.2$, $f_* = 0.8$, $f_* = 1.8$, and $f_* = 2.8$.

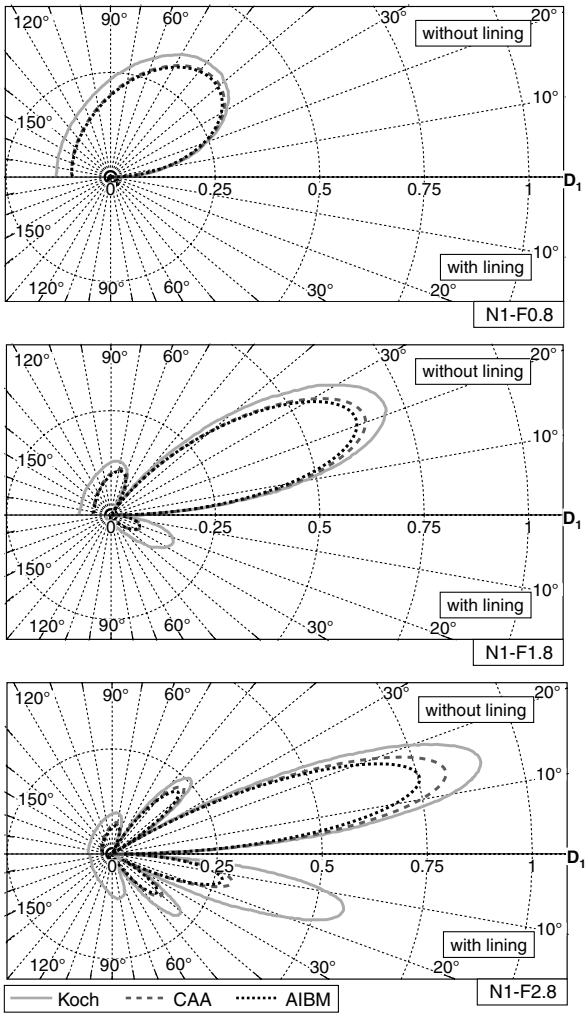

Fig. 5 Directivity factors of the first y mode D_1 [Eq. (9)]; from top to bottom, $f_* = 0.8$, $f_* = 1.8$, and $f_* = 2.8$.

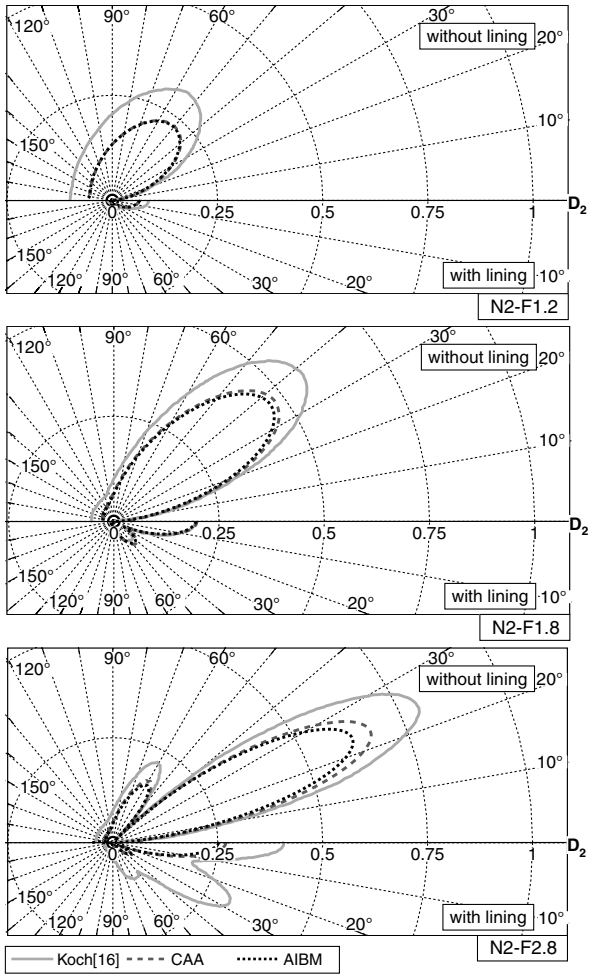

Fig. 6 Directivity factors of the second y mode D_2 [Eq. (9)]; from top to bottom, $f_* = 1.2$, $f_* = 1.8$, and $f_* = 2.8$.

CAA- and AIBM-computed intensities are smaller than the analytical, in particular when considering the lined configurations. A comparison of the AIBM far-field results with the CAA near-field results, on the other hand, shows that the AIBM-computed intensities are only slightly reduced. Thus, the proper application of the CAA method is the key to an overall accurate solution. It should be noted that the small time-step size for the lined duct cases at the same time increases the number of filtering operations for the same propagation distance. Thus, the known practical accuracy limit of approximately 7 PPW for the CAA method will not be reached for these cases. Moreover, Koch's solution did not consider a so-called Kutta condition for the trailing and leading edges of the lined surface. The current CAA result will, however, feature a partial Kutta condition at these points due to the spatial filtering of the solution. A full Kutta condition, with its high-order of accuracy concerning the following of the streamlines to the wall contour, cannot be achieved by this filtering though. This partial Kutta condition may have an influence on the solution, which cannot yet be studied in more detail. Furthermore, the source boundary condition tends to produce reflections for incoming waves close to cutoff, such that additional higher modes may be excited by the source. A combination of these effects probably leads to the observed discrepancy that also may be the underlying cause for the strong deviation of the lined duct case N2-F2.8. A mesh refinement may be applied to improve the solution quantitatively for higher frequencies. The slightly lower intensities in the aft duct region are due to the numerical induced finite duct length. Weckmüller et al. [21] showed that an extended rear duct surface minimizes the deterioration at higher radiation angles while, in return, computational costs increase.

However, the sound radiation directivities, in particular the angular accuracy of the lobes and the radiation-free regions, are predicted correctly by the hybrid method. Indeed, the radiation characteristics calculated by the CAA method, although computing only the acoustic near field, are already satisfactory enough. The absence of mean flow does not vary the radiation characteristics with increasing distance. Therefore, the AIBM gives similar results.

B. Sound Radiation from an Annular Duct with Jet Flow and a Lined Centerbody

The second benchmark problem was presented by Demir and Rienstra in 2006 [22]. It concerns the sound radiation from an annular duct with an acoustically treated centerbody. The effect of subsonic mean flow on the propagation characteristics is considered for lined and hardwalled centerbody configurations. Figure 7 shows the geometry of the problem. It consists of an annular duct: A semi-infinite outer duct with radius R_2 encompasses an infinite cylindrical centerbody with radius R_1. The outer duct consists of a hard wall from inside and outside, while the centerbody is completely hardwalled,

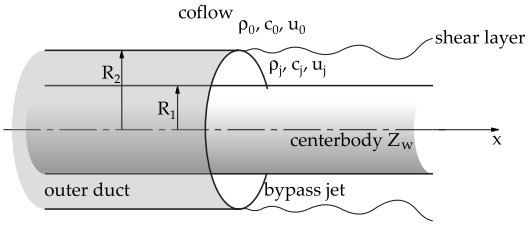

Fig. 7 Geometry of the annular duct problem according to [22].

Table 3 Specification of the studied cases of the annular duct problem

Frequency in Hz	660		1095		
Radial mode	1	2	1	2	3
Mean flow, hardwalled centerbody	MF-HC-660-1	MF-HC-660-2	MF-HC-1095-1	MF-HC-1095-2	MF-HC-1095-3
Mean flow, lined centerbody	MF-LC-660-1	MF-LC-660-2	MF-LC-1095-1	MF-LC-1095-2	MF-LC-1095-3
Without mean flow, lined centerbody	NF-LC-660-1	NF-LC-660-2	NF-LC-1095-1	NF-LC-1095-2	NF-LC-1095-3
Mean flow, lined afterbody	MF-LA-660-1		MF-LA-1095-1		

Table 4 Geometrical and physical parameters of the annular duct problem

Quantity	Value	Description
R_1	0.8 m	Inner duct radius
R_2	1.2 m	Outer duct radius
Z_w	$2-i$	Impedance of the linings
m	4	Azimuthal mode
ρ_0	1.2 kg/m^3	Ambient density
c_0	330 m/s	Ambient speed of sound
u_0	99 m/s	Mean flow velocity of the coflow
$M_{a.0}$	0.3	Mach number of the coflow
ρ_j	1.17 kg/m^3	Static density of the jet
c_j	350 m/s	Speed of sound inside the jet
u_j	175 m/s	Mean flow velocity of the jet
$M_{a.j}$	0.5	Mach number of the jet
κ	1.4	Ratio of specific heats
p_0	93,342.86 Pa	Ambient pressure
p_j	102,375 Pa	Static pressure inside the jet

Table 5 Effect of repeated smoothing steps on the shear layer thickness

Number of smoothing steps	Shear layer thickness, m
0	0.00
25	0.48
50	0.66
75	0.80

Table 6 Parameters of the EHR Model

f, Hz	R	m_{EHR}	β	T_l	ε
660	2.0	0.17456	1.8215	$2.4998 \cdot 10^{-4}$	0
1095	2.0	0.02088	1.6670	$2.4998 \cdot 10^{-4}$	0

completely lined, or partially lined from the duct exit in respective cases. The latter case is called a lined afterbody. The duct walls are assumed to be infinite thin, and the lining impedance Z_w is again of the Helmholtz type. Outside the annular duct exists an ambient flow, which is axial uniform with density ρ_0 and Mach number $M_{a.0} = \frac{u_0}{c_0}$. A shear layer emanates from the edge of the outer duct and separates this coflow from a uniform jet in the central region with density ρ_j and local Mach number $M_{a.j} = \frac{u_j}{c_j}$. Considering the cases without mean flow, the whole region consists of a homogeneous fluid with ambient properties.

A single $(m, n) = (4, n)$ mode is excited at the source and enters the region from the left between the inner and outer duct. Two frequencies, 600 and 1095 Hz, as well as the first two and three radial modes n are examined, respectively, where $n = 1$ denotes the first radial mode. The studied cases are specified in Table 3.

Table 4 lists the geometrical and physical parameters. The fluid is assumed to be an ideal diatomic gas with a ratio of specific heats of $\kappa = 1.4$. The mean ambient and jet pressures were calculated by

$$p = \frac{1}{\kappa}\rho c^2 \tag{10}$$

1. Computational Aeroacoustic Method Configuration

A modal axisymmetric approach is used in the computation [23]. The CAA solution is computed on an axisymmetric uniform grid with spacings $\Delta x = \Delta y = 0.02$ m providing a resolution of 15 PPW. Figure 8 shows the computation domain for the CAA simulations, composed of five rectangular subdomains, that consists of 204,873 grid points in total. The annular duct region is described by blocks I and II. At the boundaries to the ambience, a buffer zone of 30 grid points is attached, inside which the grid spacings are stretched by a factor of 1.05 outward to prevent grid reflections. The computation domain is colored by the nondimensional local velocity in relation to the ambient speed of sound c_0. Thus, the Mach number in the jet region is actually not the local Mach number. Depicted is also the shear layer between blocks III and IV. Demir and Rienstra [22] assume an infinite thin shear layer accompanied by an artificial discontinuous jump of the physical quantities. A model is applied to describe the passage of sound waves through the shear layer, which has a high similarity to the Ingard–Myers boundary condition at the liner. This model would add an instability for the time-domain method. Thus, the discontinuity in the mean quantities has to be smoothened for the CAA computation in order to obtain a resolved shear layer profile. A second–order Taylor filter is repeatedly applied on the base flow and the source variables to artificially thicken the shear layer. Table 5 shows the shear layer thickness depending on the executed smoothing steps. With 75 filtering iterations, the shear layer covers the complete jet width. Preliminary investigations [20] have shown that the influence of multiple filtering steps on the numerical solution can be neglected, whereas a solution can not be obtained with an infinite thin shear layer due to instability. Eventually, 50

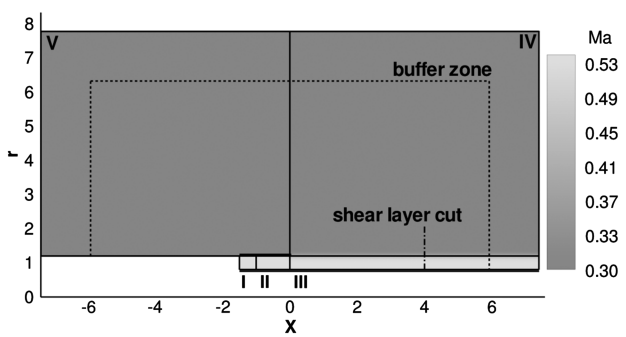

Fig. 8 CAA computation domain of the annular duct problem.

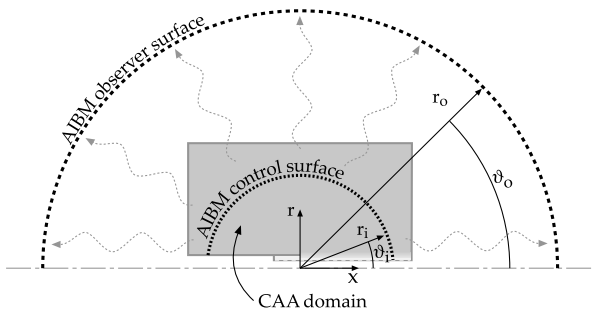

Fig. 9 AIBM control and observer surfaces of the annular duct problem.

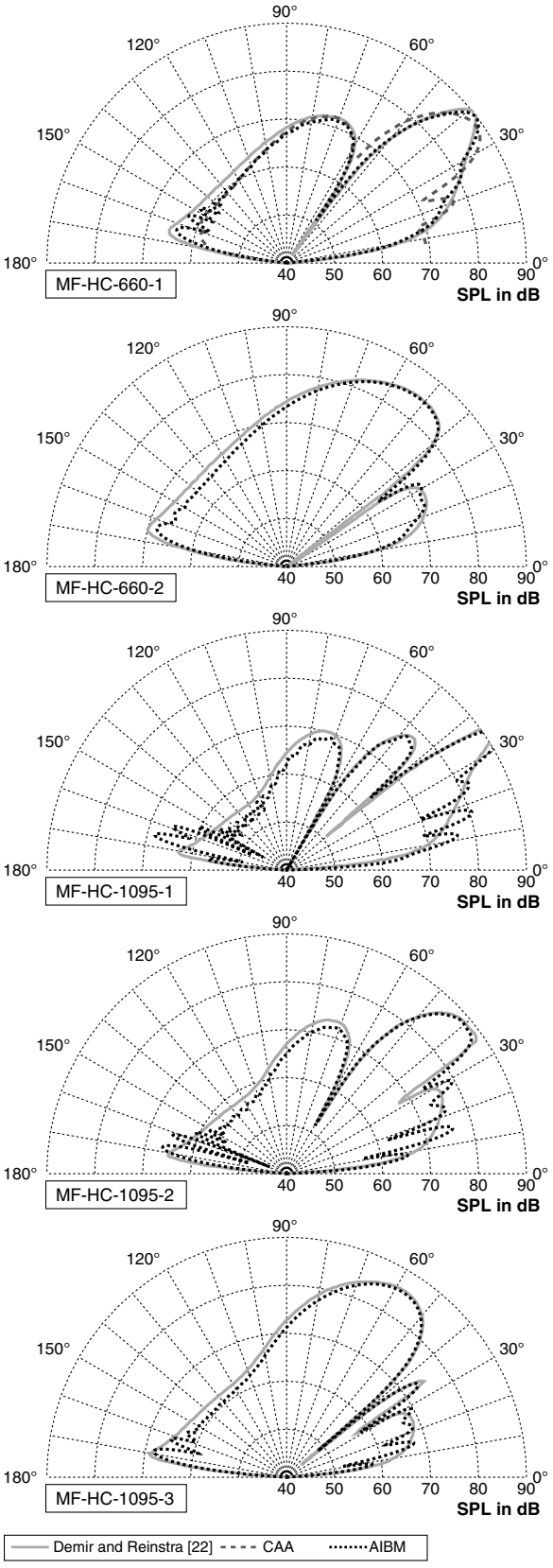

Fig. 10 SPL in decibels of the hardwalled centerbody with mean flow.

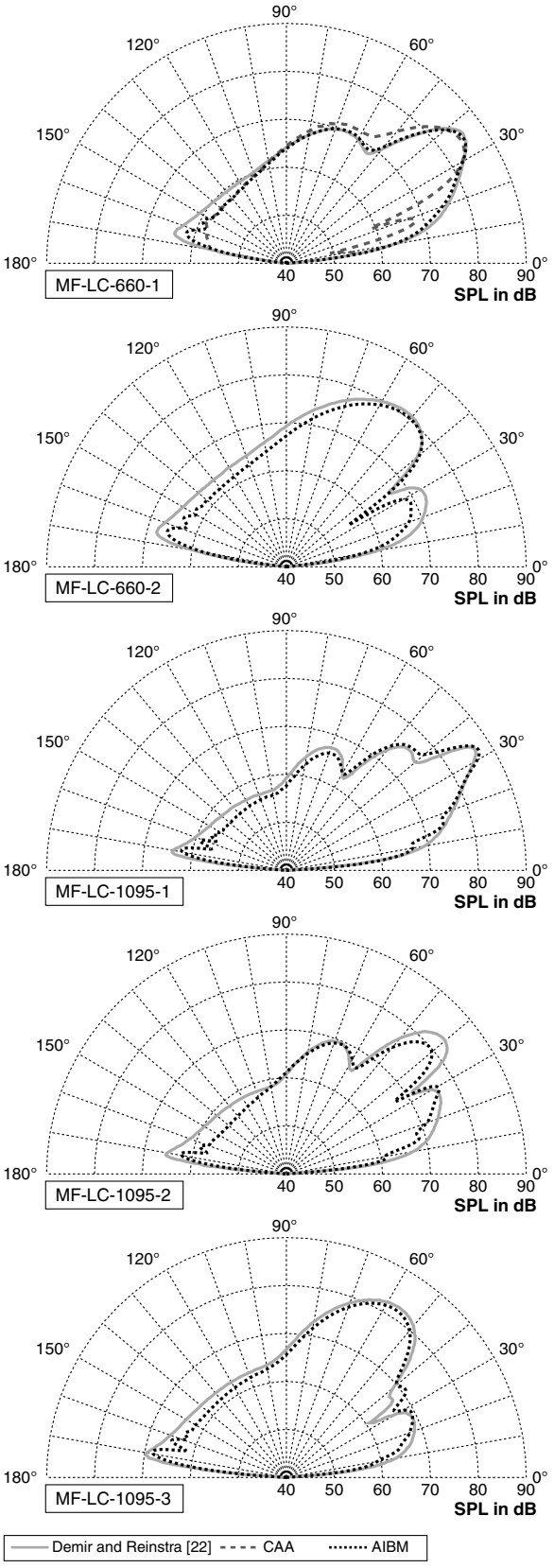

Fig. 11 SPL in decibels of the lined centerbody with mean flow.

smoothing steps were chosen for the CAA computation as a compromise between the accuracy of the numerical methods and the comparability to the analytical solutions with an infinite thin shear layer.

The sound waves enter the domain through a nonreflective sound source boundary, which is positioned on the left of block I. The impedance of the lined centerbody configurations is again modeled with the EHR model. The particular parameters to match the given impedance of $Z_w = 2 - i$ of Demir and Rienstra [22] are specified in Table 6 for the two studied frequencies. At the transition to the ambient free field, a radiation/outflow boundary condition [19] is applied.

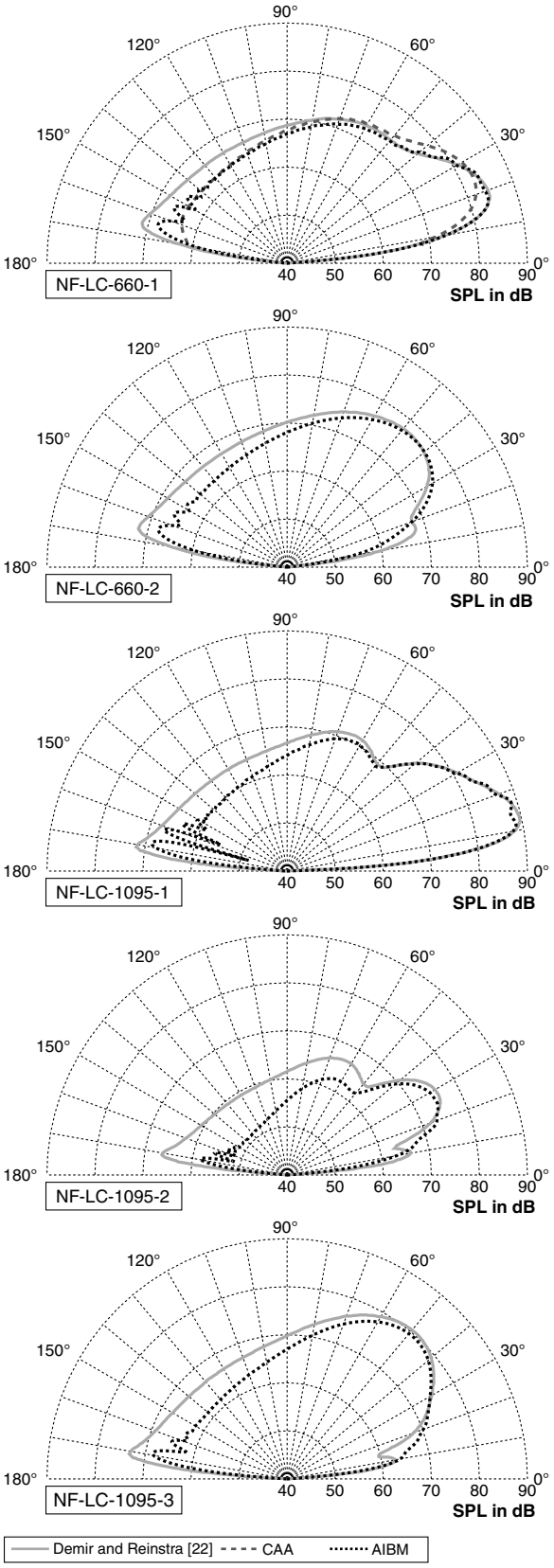

Fig. 12 SPL in decibels of the lined centerbody without mean flow.

Accurate and stable solutions were obtained with a time step of $3.64 \cdot 10^{-4}$ s for the mean flow cases and with $5.92 \cdot 10^{-5}$ s for the cases without mean flow. The modal axisymmetric CAA computations were carried out again on a 2.2 GHz AMD Opteron. Statistical stationarity is achieved after an averaged 25,000 iterations, taking approximately 15 h of computation time.

2. Acoustic Intensity-Based Method Setup

The far-field computations were carried out with the 3-D axisymmetric AIBM formulation, which is appropriate for the axisymmetric geometry of the annular duct problem. The AIBM prerequisite of an undisturbed and source-free control surface is not satisfied though. On the one hand, the infinite and semi-infinite ducts describe boundaries inside the free field, where sound waves impinge and reflect. The comparison to the analytical results of Demir and Rienstra allows us to analyze the reliability of the far-field prediction under these circumstances.

The CAA data are interpolated on a circular segment. This approach is similar to the procedure of the first problem. Based on this open control surface with radius R_i, the far field is computed on a semicircle observer surface at distance R_o from the duct exit (see Fig. 9). Analog to the procedure of the first problem studied, preliminary studies to identify the necessary number of control surface points and the control surface radius were carried out [20]. For the most accurate and effective results, an input surface radius of $R_i = 6$ m near the transition to the buffer zone, consisting of 893 points with an equal space distribution, is chosen.

According to Demir and Rienstra [22] the far field is computed and validated at $R_o = 46$ m. The observer surface consists of 500 grid points. The mean flow of the AIBM computations was set to the ambient mean flow of $c_0 = 330$ m/s. The computations are carried out on a 2.13 GHz Intel Core 2 Duo E6420 PC again, taking between 85 and 117 s.

3. Results

For validation, the SPLs of the AIBM are compared with the analytical solutions of Demir and Rienstra [22], which are calculated by means of the Wiener–Hopf technique too. For a better overview between the analytical and the numerical far-field results, the CAA results are omitted here, except for the first radial mode cases of the lower frequency. A complete comparison including the CAA results is given in Buske et al. [20]. To enable comparability, the entire sound field is normalized in the first step of the CAA postprocessing, such that the cross-sectional averaged intensity at the duct exit equals 1 W/m^2. To enable comparability with the far-field results, the CAA results, which are taken at a distance of 6 m, are scaled for the distance of 46 m.

The results of the hybrid method, depicted in Figs. 10–13, show in general a very good agreement with the analytical solution for all

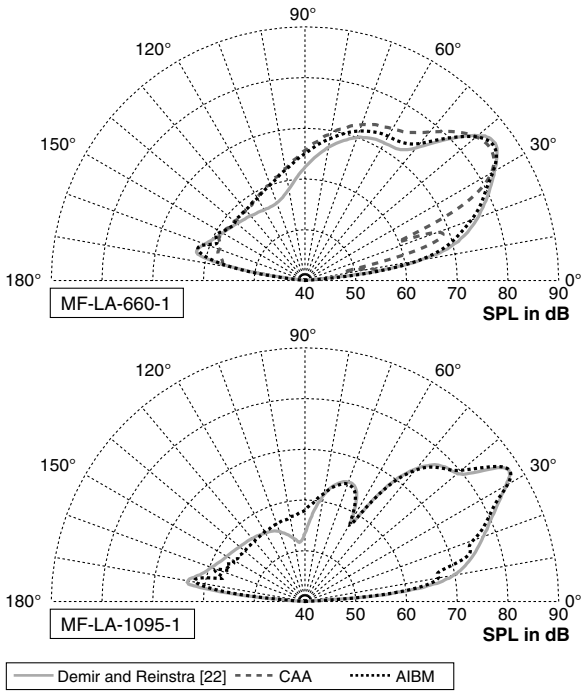

Fig. 13 SPL in decibels of the lined afterbody with mean flow.

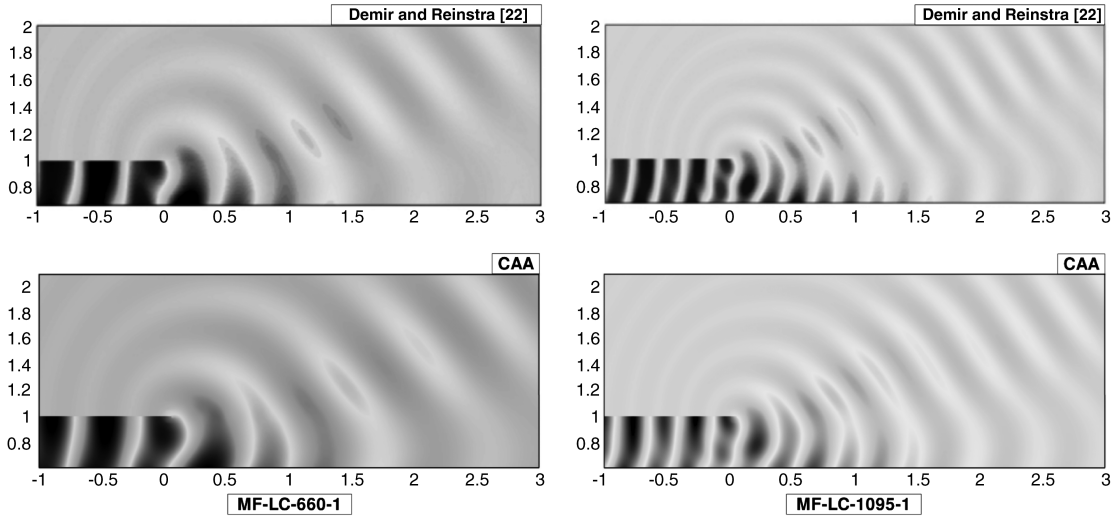

Fig. 14 Instantaneous pressure contours of the acoustic near field.

cases. The CAA results show near-field influences, as the main lobes are deflected to some higher degrees, and the shear layer adds an additional lobe especially for the lined centerbody (see Fig. 11). Furthermore, the scaled SPLs of the CAA method are underpredicted at upstream angles compared with the analytical far-field solutions, in particular when no mean flow is considered (see for instance, Fig. 12). This divergence was also observed at the study of Koch's problem [16] and seems to be a characteristic inaccuracy due to the limited size of the CAA domain. An extended computation domain to the aft region and a refined grid may improve the solution as previously mentioned. The application of the far-field AIBM ceases the near-field effects of the CAA. The directivity of the main lobes agree exceptionally well with the analytical solution. Only the radiation-free angles are less distinctive. Undulations of the AIBM occur mainly above 150° and in the critical regions near the duct walls due to the missing AIBM input data from inside the duct. Thus, the AIBM has to guess the sound field in that angular direction. The shear layer of the hardwalled configurations (see Fig. 10) generates additional spurious oscillations at upstream angles, because the inhomogeneous flowfield does not comply with the AIBM requirements. Yet, the main sound radiation characteristics are reproduced correctly by the hybrid approach, with major deviations in the SPL of not more than 4 dB in cases where mean flows are present and 10 dB, at most, for the cases without mean flow.

Demir and Rienstra [22] also provide pressure contour plots of the near field for cases MF-LC-660-1 and MF-LC-1095-1. In Fig. 14, they are compared with the CAA-computed instantaneous pressure perturbations. Although the phase angle of the instantaneous plots is not exactly the same, the propagation characteristics inside and outside the annular duct are found in reasonable agreement.

IV. Conclusions

A zonal approach combining a finite difference time-domain CAA method based on the DRP and an AIBM has been validated. The CAA method incorporates a broadband time-domain impedance model, which is based on the EHR model and can include a model for the base flow effects on the impedance of the lined surface by the Ingard–Myers boundary condition. The AIBM is characterized by the possibility of using open control surfaces, which allow us to exclude regions with large flow gradients in the average field from the exchange surface. The comprehensive comparison to the analytical solution for the 2-D and axisymmetric geometries and various mean flow conditions validates the accuracy of the whole method by correct predictions for hardwall, as well as softwall, acoustic radiation. The effectiveness of the AIBM, in particular, makes this approach advantageous compared with classical integration far-field methods.

Acknowledgments

The current research is part of the LiMiT project (liner impedance modeling in the time domain with flow), which was funded by the German Research Foundation (DFG). The exchange with the Michigan State University, which made this excellent example of an international research cooperation possible, was funded by the German Academic Exchange Service (DAAD). The computations were mainly carried out at the high-performance scientific computing facilities of Michigan State University. Finally, the authors want to acknowledge the excellent works of Koch, Demir, and Rienstra, who provided the analytical basis for the current validation.

References

[1] Hardin, J. C., and Lemkin, S. L., "Aeroacoustic Computation of Cylinder Wake Flow," *AIAA Journal*, Vol. 22, No. 1, 1984, pp. 51–57. doi:10.2514/3.48418

[2] Zhang, X., Chen, X. X., Morfey, C. L., and Nelson, P. A., "Computation of Spinning Modal Radiation from an Unflanged Duct," AIAA Paper 2002-2475, 2002.

[3] Zhang, X., Chen, X. X., Morfey, C. L., and Nelson, P. A., "Computation of Spinning Modal Radiation from an Unflanged Duct," *AIAA Journal*, Vol. 42, No. 9, Sept. 2004, pp. 1795–1801; also AIAA Paper 2002-2475, 2002. doi:10.2514/1.890

[4] Rienstra, S. W., "Impedance Models in Time Domain, Including the Extended Helmholtz Resonator Model," AIAA Paper 2006-2686, May 2006.

[5] Richter, C., Thiele, F., Li, X., and Zhuang, M., "Comparison of Time-Domain Impedance Boundary Conditions by Lined Duct Flows," AIAA Paper 2006-2527, May 2006.

[6] Richter, C., and Thiele, F., "The Stability of Time Explicit Impedance Models," AIAA Paper 2007-3538, May 2007.

[7] Richter, C., Thiele, F., Li, X. D., and Zhuang, M., "Comparison of Time-Domain Impedance Boundary Conditions for Lined Duct Flows," *AIAA Journal*, Vol. 45, No. 6, June 2007, pp. 1333–1346. doi:10.2514/1.24945

[8] Yu, C., Zhou, Z., and Zhuang, M., "An Acoustic Intensity-Based Inverse Method," *Journal of the Acoustical Society of America*, Vol. 123, No. 4, 2008, pp. 1892–1901. doi:10.1121/1.2875046

[9] Yu, C., Zhou, Z., Zhuang, M., Li, X., and Thiele, F., "Effective Far-Field Acoustic Prediction Method and Its Computational Aeroacoustics Applications," *AIAA Journal*, Vol. 47, No. 2, Feb. 2009, pp. 410–417. doi:10.2514/1.39009

[10] Yu, C., Zhou, Z., and Zhuang, M., "Acoustic Intensity-Based Method for Acoustic Radiations in a Uniform Flow," *Journal of the Acoustical Society of America*, Vol. 126, No. 5, 2009, pp. 2198–2205. doi:10.1121/1.3224764

[11] Tam, C. K. W., and Webb, C., "Dispersion-Relation-Preserving Finite Difference Schemes for Computational Aeroacoustics," *Journal of*

Computational Physics, Vol. 107, No. 2, Aug. 1993, pp. 262–281.
doi:10.1006/jcph.1993.1142

[12] Stanescu, D., and Habashi, W., "2N-storage Low-dissipation and Low-dispersion Runge-Kutta Schemes for Computational Aeroacoustics," *Journal of Computational Physics*, Vol. 143, No. 2, July 1998, pp. 674–681.
doi:10.1006/jcph.1998.5986

[13] Schoenwald, N., Panek, L., Richter, C., and Thiele, F., "Investigation of Sound Radiation from a Scarfed Intake by CAA-FWH Simulations Using Overset Grids," AIAA Paper 2007-3524, May 2007.

[14] Panek, L., Schoenwald, N., Richter, C., and Thiele, F., "Simulation of the Rearward Propagation of Fan Noise through a Long Cowl Aero-Engine," AIAA Paper 2008-2820, 2008.

[15] Myers, M. K., "On the Acoustic Boundary Condition in the Presence of Flow," *Journal of Sound and Vibration*, Vol. 71, No. 3, Aug. 1980, pp. 429–434.
doi:10.1016/0022-460X(80)90424-1

[16] Koch, W., "Radiation of Sound from a Two-Dimensional Acoustically Lined Duct," *Journal of Sound and Vibration*, Vol. 55, No. 2, Nov. 1977, pp. 255–274.
doi:10.1016/0022-460X(77)90598-3

[17] Ko, S.-H., "Sound Attenuation in Lined Rectangular Ducts and its Application to the Reduction of Aircraft Engine Noise," *Journal of the Acoustical Society of America*, Vol. 50, No. 6, Part 1, Dec. 1971, pp. 1418–1432.
doi:10.1121/1.1912784

[18] "U.S. Standard Atmosphere, 1976," U. S. Government Printing Office, Washington, D. C., 1976.

[19] Bogey, C., and Bailly, C., "Three-Dimensional Non-Reflective Boundary Conditions for Acoustic Simulations: Far Field Formulation and Validation Test Cases," *Acta Acustica United with Acustica*, Vol. 88, 2002, pp. 463–471.

[20] Buske, C., Richter, C., Thiele, F., Yu, C., and Zhuang, M., "Validation of a Zonal Method Computing the Sound Radiation from Lined Ducts," AIAA Paper 2009-3169, May 2009.

[21] Weckmueller, C., Guerin, S., and Richter, C., "Numerical Investigation of Geometry and Mean Flow Effects on Acoustic Radiation from a Duct Inlet," AIAA Paper 2007-3535, May 2007.

[22] Demir, A., and Rienstra, S. W., "Sound Radiation from an Annular Duct with Jet Flow and a Lined Centerbody," AIAA Paper 2006-2718, May 2006.

[23] Li, X., Schemel, C., Michel, U., and Thiele, F., "Azimuthal Sound Mode Propagation in Axisymmetric Flow Ducts," *AIAA Journal*, Vol. 42, No. 10, Oct. 2004, pp. 2019–2027.
doi:10.2514/1.11952

C. Bailly
Associate Editor